Phys. Status Solidi RRL **6**, No. 2, 92–94 (2012) / **DOI** 10.1002/pssr.201105498

pss +++rapid research letters+++
www.pss-rapid.com

Tunable magnetic anisotropy of $CoFe_2O_4$ nanopillar arrays released from $BiFeO_3$ matrix

Zhiguang Wang [*, 1], **Ravindranath Viswan**[1], **Bolin Hu**[2], **V. G. Harris**[2], **Jie-Fang Li**[1], **and D. Viehland**[1]

[1] Department of Materials Science and Engineering, Virginia Tech, 306 Holden Hall, Blacksburg, Virginia 24061, USA
[2] Department of Electrical and Computer Engineering, Northeastern University, Boston, Massachusetts 02115, USA

Received 24 October 2011, revised 10 November 2011, accepted 11 November 2011
Published online 17 November 2011

Keywords self-assembly, thin films, magnetic anisotropy, $CoFe_2O_4$ nanopillars, magnetic force microscopy

* Corresponding author: e-mail zgwang@vt.edu, Phone: +01 540 232 6928, Fax: +01 540 231 8919

We deposited epitaxial $BiFeO_3$–$CoFe_2O_4$ (BFO–CFO) self-assembled thin films on (001) $SrTiO_3$ (STO) substrates. We find that a combined annealing and etching process could remove the BFO matrix, thereby resulting in free-standing CFO nanopillar arrays. Scanning electron and atomic force microscopies showed well separated CFO nanopillars, which were very similar to the original CFO ones in the self-assembled structure. Finally, comparison of the magnetic hysteresis loops before and after removal of the BFO matrix showed a significant decrease of the coercive field and a dramatic decrease in the strain dominated magnetic anisotropy.

1 Introduction Complex oxides are an extremely rich family of compounds displaying a remarkable range of functional properties, including superconductivity as well as ferroic orders such as magnetism and ferroelectricity [1]. Interfaces in such complex oxide thin films are of particular interest because specific strain or polar boundary conditions can lead to additional interface-induced effects: ultra-high carrier mobility and concentration at room temperature in 2D interface electron gases [2]; interface-induced high temperature superconductivity [3]; and enhanced interface magnetism [4]. However, these interfacial structures are in the form of conventional hetero-epitaxial multilayers, where the interface is buried at the bottom of the film making it difficult to probe it by direct measurements. The emergence of self-assembled thin film structures, on the other hand, offers interfaces that intersect the thin film surface; thus, they could be easily probed, offering promise in fabrication of 3D devices.

Since the observation of phase separation in the (La,Ca)MnO_3–MgO system [5], epitaxial growth of nanoscale self-assembled structures has been extensively investigated in other systems. Segregation of perovskite–spinel systems has been explored, showing a series of nanopillars embedded in matrix structures [6–13]. Nanoarrays of ferromagnetic materials are important for the fabrication of magnetic recording and spintronic devices. Traditional lithography was developed for patterning of semiconductors, and there are only a few reports on patterned oxide magnets by this method due to their chemical inertness [14]. To solve this problem, anodized aluminum oxide templates have been used for the fabrication of high density CFO nanoarrays [14–16].

Here, a process that combines pulsed laser deposition (PLD) of self-assembled $BiFeO_3$–$CoFe_2O_4$ (BFO–CFO), thermal evaporation treatment and a subsequent etching process has been applied to self-assembled BFO–CFO on $SrRuO_3$/$SrTiO_3$ (SRO/STO) heterostructures. This process then allows for the fabrication of CFO nanopillar arrays and tailoring of the magnetic anisotropy [17, 18].

2 Experimental details We deposited $65BiFeO_3$–$35CoFe_2O_4$ epitaxial thin films by pulsed laser deposition (KrF excimer laser, $\lambda = 248$ nm) on (001) oriented SRO buffered STO single crystal substrates. The crystal structure of the films was measured using a Philips X'pert high resolution X-ray diffractometer designed for single crystalline samples. The surface morphologies of the self-assembled films were studied using a LEO Zeiss 1550

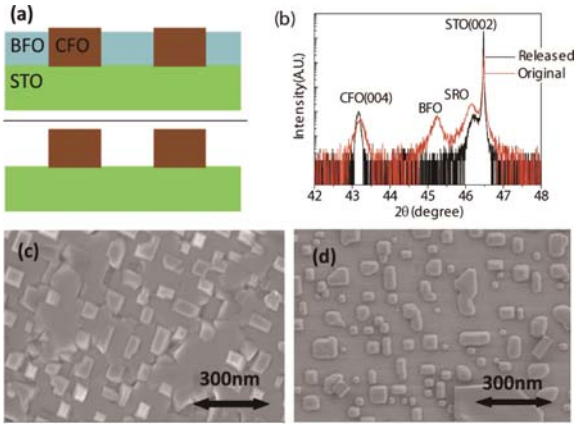

Figure 1 (online colour at: www.pss-rapid.com) (a) Schematics of the releasing process. (b) XRD line scan profiles, before and after release of BFO. (c) and (d) SEM top view images of BFO–CFO before and after release, respectively.

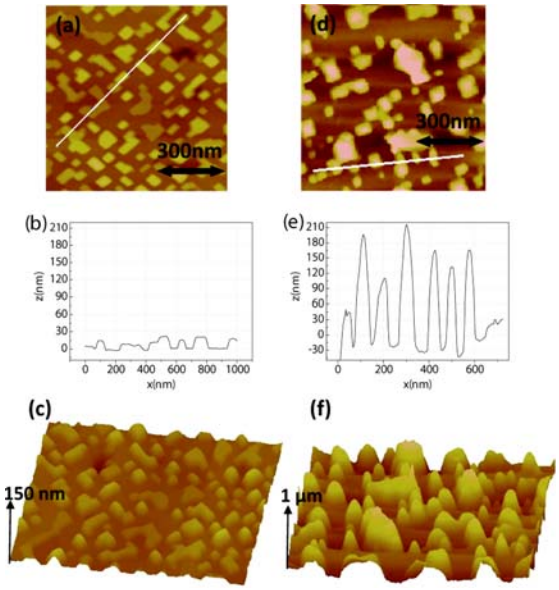

Figure 2 (online colour at: www.pss-rapid.com) Topographic AFM images of BFO–CFO self-assembled structure before (a) and after (d) release. (b) and (e) Line profiles taken from selected areas in (a) and (d), respectively. (c) and (f) 3D AFM topography images (1 μm × 1 μm) of (a) and (d), respectively.

Schottky field-emission scanning electron microscopy (SEM). The topography and magnetic domain structures were characterized by a Veeco SPI 3100 atomic force microscopy (AFM) and magnetic force microscopy (MFM). Magnetic hysteresis loops were measured with a Lakeshore 7300 series vibrating sample magnetometer (VSM) system at room temperature.

3 Results and discussion Figure 1(a) shows a preparation schematics. Composite targets of 65BFO–35CFO were used for the deposition of the self-assembled BFO–CFO composite thin film precursors. The two immiscible phases decompose naturally during growth due to different surface energy anisotropies between the spinel CFO and perovskite BFO phases [9]. The BFO phase can easily wet on (100) oriented SRO/STO forming a matrix, whereas the CFO phase nucleates and forms nanopillars with a rectangular top surface. Bulk CFO is ferromagnetic with a cubic Fm3m structure (a_{CFO} = 8.392 Å), while bulk BFO is ferroelectric with a pseudocubic structure (a_{BFO} = 3.96 Å). Thus, CFO is under compressive strain from the BFO matrix in a self-assembled structure: as $a_{CFO} > 2a_{BFO}$. This compressive strain can be estimated as 0.26% by calculating the *c*-axis lattice change from the right shift of the CFO (004) diffraction peak relative to the single crystal value: see XRD line scan (red curve) in Fig. 1(b). We then annealed the samples at 900 °C in air for three hours to evaporate Bi, leaving only the iron oxide phase which was then etched off using a dilute acid. Accordingly, we released the CFO nanopillars from the BFO matrix. Furthermore, XRD line scans (black curve) show the disappearance of the BFO peaks, and a sharper left-shifted CFO (004) peak. The residual strain in the CFO phase was decreased to 0.16%. The full-width at half-maximum (FWHM) of the CFO (004) peak was also decreased (from 0.2° to 0.15°), due to the relaxation of the strain from BFO phase. Figures 1(c) and (d) show top view SEM images for BFO–CFO self-assembled structures before and after removal of the BFO matrix, respectively. Figure 1(c) clearly shows self-assembled CFO nanopillars with a rectangular morphology embedded in a BFO matrix. The size of the CFO nanopillars was about 80 nm. After annealing (see Fig. 1d), one can clearly see free-standing CFO nanostructures of nearly the same size. These results demonstrate that we preserve the CFO nanostructure after removing the BFO matrix by annealing and etching.

Figure 2 shows AFM images that illustrate the 3D topography of the CFO nanoarray structures. Part (a) shows a topography image of the BFO–CFO thin films surface, for which a line profile (taken along the white line in Fig. 2a) is given in part (b). We can see that the CFO nanopillars are slightly higher than the BFO matrix and that topography relief is less than 20 nm in height: this demonstrates a smooth surface. The corresponding 3D image is shown in part (c), where we can observe well-separated CFO nanopillars with a relatively smooth top surface embedded in a BFO matrix. We then performed similar measurements after removal of the BFO matrix. The height of the CFO nanopillar features was increased to nearly 200 nm, which was close to the thickness of the original BFO–CFO thin films. This shows that the BFO matrix was removed and that the CFO nanopillars are free-standing on SRO/STO substrates. Part (f) gives a 3D image of the free-standing CFO nanoarray structure.

Finally, we studied the spin configuration and magnetic domain distribution of the CFO nanopillars by VSM and MFM, as shown in Fig. 3. Part (a) shows the *M*–*H* loops of an as-prepared BFO–CFO self-assembled thin film. When normalized to the volume fraction of

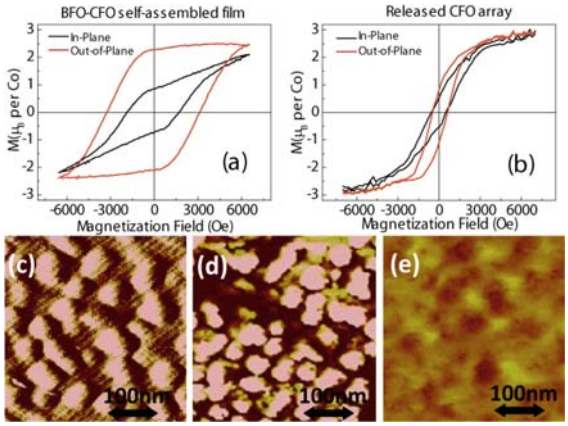

Figure 3 (online colour at: www.pss-rapid.com) Magnetic hysteresis loops of BFO–CFO self-assembled nanostructures before (a) and after (b) release. (c) MFM image of as prepared BFO–CFO; and AFM (d) and MFM (e) images of released CFO nanopillars.

CFO (~37%), the film had a saturation magnetization of $M_s \approx 2.4\mu_B$ per Co. The $M-H$ loop in the out-of-plane direction was square-like with a coercive field of ~3 kOe. The remnant magnetization was $M_r \approx 2.15\mu_B$ per Co. This shows that most of the magnetic moments that have been aligned out-of-plane remained in the same direction after removal of H. In contrast, the $M-H$ loop in the in-plane direction was relatively slim and required a much larger magnetic field to achieve saturation.

However, the magnetostrictive anisotropy will be greatly decreased by release of the CFO nanopillars from the BFO matrix. As a result, the released CFO nanopillars should exhibit properties much like unstrained bulk CFO single crystals: with a decreased coercive field [14, 15] and reduced anisotropy between in-plane and out-of-plane directions. One point to be noted after removal of the BFO matrix is that M_s increased from about $2.4\mu_B$ to $3\mu_B$ per Co: which can be explained by a change in the surface spin state induced by exchange coupling between ferromagnetic CFO and antiferromagnetic BFO interfaces. After release from the BFO matrix, this spin coupling is destroyed and the surface area of CFO can then contribute more to the magnetization, resulting in a larger saturation value. Figure 3(c) shows the MFM image of BFO–CFO self-assembled thin films. A single domain state can be seen in each pillar. Figures 3(d) and (e) show AFM and MFM images of released CFO nanopillars. A lower remnant magnetization in the out-of-plane direction resulted in a 'fuzzy' MFM image; in addition, a dark–bright contrast can be seen within individual CFO nanopillars, revealing that multi-domain states emerged after release. Both the $M-H$ loop and MFM results reveal that the magnetic state is less stable after the release for the CFO nanopillars.

In summary, we have deposited well-distributed BFO–CFO self-assembled epitaxial layers on SRO buffered STO substrates, and then subsequently used annealing and etching to release the CFO nanopillar arrays from the BFO matrix. XRD and AFM demonstrated good epitaxy for the CFO phases and that the original CFO nanopillar array morphology was maintained after annealing–etching. Finally, the magnetic hysteresis loop and MFM measurements demonstrated that removal of the BFO matrix could greatly decrease the strain and spin coupling at the CFO/BFO interfaces, thus reducing the magnetic anisotropy of the CFO phase. A change in both coercive field and saturation magnetization strongly indicates the possibility of tuning the magnetic properties of the CFO phase by strain.

Acknowledgements We would like to gratefully acknowledge financial support from the U.S. Department of Energy and the Air Force Office of Scientific Research.

References

[1] J. L. MacManus-Driscoll, Adv. Funct. Mater. **20**, 2035 (2010).
[2] A. Ohtomo and H. Y. Hwang, Nature **427**, 423 (2004).
[3] G. Logvenov, A. Gozar, and I. Bozovic, Science **326**, 699 (2009).
[4] H. Yamada, Y. Ogawa, Y. Ishii, H. Sato, M. Kawasaki, H. Akoh, and Y. Tokura, Science **305**, 646 (2004).
[5] O. I. Lebedev, J. Verbeeck, G. Van Tendeloo, O. Shapoval, A. Belenchuk, V. Moshnyaga, B. Damaschke, and K. Samwer, Phys. Rev. B **66**, 104421 (2002).
[6] H. Zheng, J. Wang, S. E. Lofland, Z. Ma, L. Mohaddes-Ardabili, T. Zhao, L. Salamanca-Riba, S. R. Shinde, S. B. Ogale, F. Bai, D. Viehland, Y. Jia, D. G. Schlom, M. Wuttig, A. Roytburd, and R. Ramesh, Science **303**, 661 (2004).
[7] F. Zavaliche, H. Zheng, L. Mohaddes-Ardabili, S. Y. Yang, Q. Zhan, P. Shafer, E. Reilly, R. Chopdekar, Y. Jia, P. Wright, D. G. Schlom et al., Nano Lett. **5**, 1793 (2005).
[8] I. Levin, J. H. Li, J. Slutsker, and A. L. Roytburd, Adv. Mater. **18**, 2044 (2006).
[9] H. Zheng, Q. Zhan, F. Zavaliche, M. Sherburne, F. Straub, M. P. Cruz, L. Q. Chen, U. Dahmen, and R. Ramesh, Nano Lett. **6**, 1401 (2006).
[10] F. Zavaliche, T. Zhao, H. Zheng, F. Straub, M. P. Cruz, P. L. Yang, D. Hao, and R. Ramesh, Nano Lett. **7**, 1586 (2007).
[11] S. Q. Ren, R. M. Briber, and M. Wuttig, Appl. Phys. Lett. **93**, 173507 (2008).
[12] B. Liu, T. Sun, J. He, and V. P. Dravid, ACS Nano **4**, 6936 (2010).
[13] Z. Wang, Y. Yang, R. Viswan, J. Li, and D. Viehland, Appl. Phys. Lett. **99**, 043110 (2011).
[14] X. S. Gao, L. F. Liu, B. Birajdar, M. Ziese, W. Lee, M. Alexe, and D. Hesse, Adv. Funct. Mater. **19**, 3450 (2009).
[15] X. S. Gao, B. J. Rodriguez, L. F. Liu, B. Birajdar, D. Pantel, M. Ziese, M. Alexe, and D. Hesse, ACS Nano **4**, 1099 (2010).
[16] X. Lu, Y. Kim, S. Goetze, X. Li, S. Dong, P. Werner, M. Alexe, and D. Hesse, Nano Lett. **11**, 3202 (2011).
[17] Y. Lin, A. Böker, J. He, K. Sill, H. Xiang, C. Abetz, X. Li, J. Wang, T. Emrick, S. Long, Q. Wang, A. Balazs, and T. P. Russell, Nature **434**, 55 (2005).
[18] Y. Wu, Y. Matsushita, and Y. Suzuki, Phys. Rev. B **64**, 220404(R).

